Ultrafast relaxation dynamics of the antiferrodistortive phase in Ca doped $SrTiO_3$

-Supplementary Information-

30.04.2018

M. Porer[1], M. Fechner[2,3], E. Bothschafter[1], L. Rettig[1,4], M. Savoini[1,5], V. Esposito[1], J. Rittmann[1], M. Kubli[5], M. J. Neugebauer[5], E. Abreu[5], T. Kubacka[5], T. Huber[5], G. Lantz[5], S. Parchenko[1], S. Grübel[1], A. Paarmann[4], J. Noack[6], P. Beaud[1], G. Ingold[1], U. Aschauer[7], S. L. Johnson[5], U. Staub[1]

[1] *Swiss Light Source, Paul Scherrer Institute, 5232 Villigen-PSI, Switzerland*
[2] *Max Planck Institute for the Structure and Dynamics of Matter, CFEL, 22761 Hamburg, Germany*
[3] *Materials Theory, ETH Zürich, 8093 Zürich, Switzerland*
[4] *Department of Physical Chemistry, Fritz Haber Institute of the Max Planck Society, 14195 Berlin, Germany*
[5] *Institute for Quantum Electronics, ETH Zürich, 8093 Zürich, Switzerland*
[6] *Department of Inorganic Chemistry, Fritz Haber Institute of the Max Planck Society, 14195 Berlin, Germany*
[7] *Department of Chemistry and Biochemistry, University of Bern, 3012 Bern, Switzerland*

1. Structure factor of the (1.5 0.5 0.5) superlattice reflection

The structure factor F_{hkl} of the (1.5 0.5 0.5) superlattice reflection ((2 1 1) in the I4/mcm space group) of $SrTiO_3$ amounts to:

$$F_{\frac{3}{2}\frac{1}{2}\frac{1}{2}} = 4f_{O2-} \cdot (\sin(2\pi \cdot u) + \sin(6\pi \cdot u)) \approx 32\pi f_{O2-} u + \mathcal{O}(u^2)$$

with f_{O2-} the atomic form factor of the oxygen 8h sites and u the fractional lattice displacement in I4/mcm unit cell coordinates.

With u~φ, the intensity depends on u and φ as

$$I_{\frac{3}{2}\frac{1}{2}\frac{1}{2}} \propto F^2_{\frac{3}{2}\frac{1}{2}\frac{1}{2}} \propto \varphi^2 + \mathcal{O}(\varphi^4)$$

This approximation of a square dependence holds for $\varphi \ll \pi/6$, which is given for realistic values of $\varphi \lesssim 0.035$ (~2°) [18].

2. Temperature dependence of the soft-mode frequency

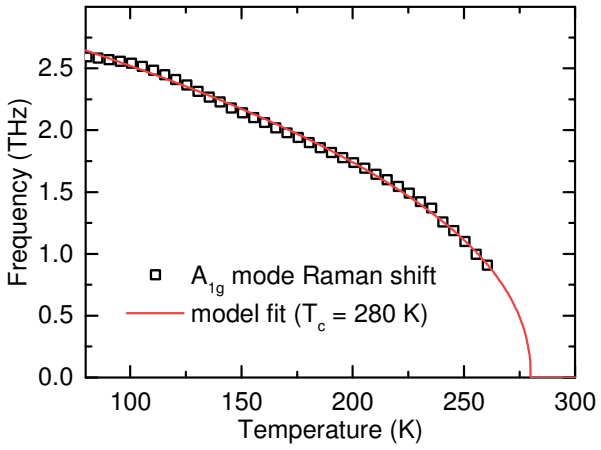

Figure S1 Frequency of the antiferrodistortive soft mode in $Sr_{0.97}Ca_{0.03}TiO_3$ as a function of temperature as measured by Raman spectroscopy. A power law fit reveals a critical temperature of T_c = 280 K for the structural phase transition. Measurements were performed at the Fritz Haber Institute, Berlin.

3. Fluence and temperature dependence of the fast relaxation time constant

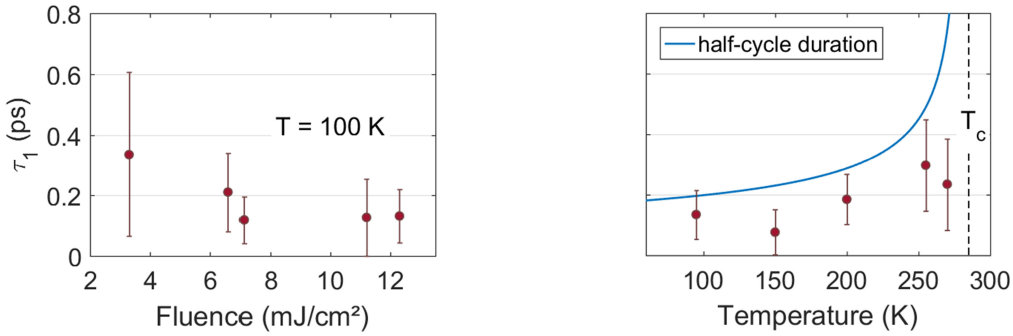

Figure S2 Fast decay time constant τ_1 of the lattice displacement u extracted from the dynamics of the (1.5 0.5 0.5) reflection intensity as (a) function of excitation fluence Φ at a T = 100 K and (b) as function of T at Φ = 6 mJ/cm².

4. Exclusion of an order-disorder transition scenario

As discussed in the main text, we can exclude a scenario in which the intensity reduction of the superlattice reflection can be attributed purely to the Debye-Waller factor of a thermally heated and equilibrated crystal lattice. For the structural transition studied here, one may further consider the implications of selective heating of the A_{1g} soft-mode or the oxygen 8h sites involved in the structural transition. Besides a favored population of the low frequency modes including the soft mode given by the Bose-Einstein statistics, depending on the mode-selective electron-phonon couplings, cooling of photoexcited carriers via phonon emission could in principle favor scattering into the soft mode branch. Such effects would lead to a temporarily increased thermal average displacement of the oxygen 8h sites that may rapidly reduce the intensity of the superlattice reflection and persist longer than captured by our experimental time window of a few picoseconds.

To test such a scenario, we reference the SL reflection intensity against the intensity of the structural (1 3 1) reflection, which exhibits a similar sensitivity to the thermal displacement of the 8h oxygens.

Figure S3 compares the expected influence of such thermal dislocation on the intensities of the superlattice (1.5 0.5 0.5) and the structural (1 3 1) reflections for two scenarios: First, we assume a O 8h dislocation approximately along the soft mode coordinate by elongating the thermal ellipsoid along the mode coordinate for small φ (left inset). Second, we assume an isotropic thermal displacement within the ab-plane (right inset). In either scenario, we find that a thermally induced reduction of the superlattice reflection (green curves) would imply a comparable drop in the measured structural reflection (red curves).

In our experiment, photoexcitation with Φ = 6 mJ/cm^2 yields no measurable change in the (1 3 1) reflection intensity within an error of 0.5% and in a time window of 5 ps after excitation.

Thus, we can exclude a scenario where the drop in the superlattice intensity can be attributed to a rapid thermal dislocation of the oxygen 8h sites, comparable to an order-disorder transition of the structural superlattice.

We note that dislocation of the oxygens along softened E_g modes [33] (oxygen motions along the c-axis) does not significantly affect the expected intensity of the superlattice reflection (not shown).

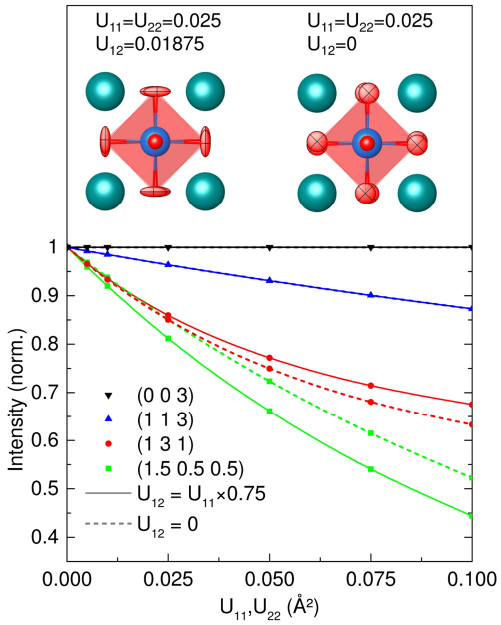

Figure S3 Expected intensity reduction of select x-ray reflections at 7.1 keV upon selective thermal heating. The abscissa represents the in plane thermal dislocation of the oxygen 8h sites. All components of the other thermal ellipsoid $U_{ij(i\leq j)}$ are zero unless stated otherwise. Insets: Thermal ellipsoids (90% probability) of the 8h oxygen sites viewed along the c-axis for dislocation mainly along the soft mode coordinate (left) and isotropic within the ab-plane (right). Structure factor calculations and visualizations are performed with VESTA [23].

5. Doping dependence of the double-well potential coefficients

To determine the doping dependent coefficients of Eq. (1) we perform first-principle computations of the phonon band structure utilizing the approach and numerical setting of Ref. [30]. We determine the quadratic and quartic coefficients by modulating the structure along the eigenvector of the R-point phonon mode. By modulating the structure with the previously computed soft mode eigenvector we calculate the total energy of the system as a function of the mode amplitude. Finally, we fit the obtained energy landscape by a polynomial expression given in Eq. (1). In Fig. S4, we show the gained square and quartic coefficients as a function of doping. Whereas the quartic term is nearly unaffected by doping, we found a linear increase in the square factor.

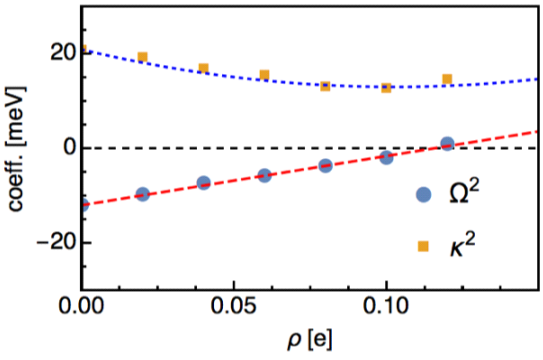

Figure S4: Change of the potential coefficients in Eq. (1) by hole doping.

6. Details of the TDDFT computations

We perform the TDDFT computations utilizing the implementations within the ELK code [32]. The electromagnetic field of the pump pulse is described by a time dependent vector potential.

We performed our computations for the cubic structure of $SrTiO_3$ with $a = 3.9$ Å using as approximation for the exchange correlation functional the local density approximation (LDA). The numerical parameters for the time dependent computations have been fixed after thorough convergence tests. We use explicitly: 7x7x7 k-point mesh to sample the Brillouin zone, a plane-wave cutoff within the interstitial of $|G + k|_{max} R_{MT}^{avg} = 7.5$ with the average muffin tin Radius $R_{MT}^{avg} = 0.98$ Å, we truncate the potential and density at $G_{max} = 20/a_0$, the maximum angular momentum for the local basis within the muffin tin is set to $l_{max} = 10$ for potential and wavefunction. Moreover, we add a total of 100 empty states to our basis to properly describe the excited states. For all not explicit listed parameters, we use the settings for high quality computations in Elk as triggered by "highq=.true.".

Firstly, we perform a static regular DFT calculation of $SrTiO_3$ to determine its ground state electronic properties. Fig. S5 shows the electronic band structure of $SrTiO_3$ along selected symmetry lines within the first Brillouin zone. From this computation, we deduce the indirect LDA DFT band gap of $SrTiO_3$ to be 2 eV, which is lower than its experimental value of 3.25 eV [25]. Please note, that for the time-dependent calculation we have to take into account the deficiency of the LDA band gap to perform realistic computations.

We characterize the pump pulse in our computations by a Gaussian envelope pulse carrying a central frequency corresponding to 2 eV and with an FWHM of 80 fs. The amplitude of the pulse is adjusted to give similar fluence values a used in the experiment. Utilizing these values, we perform TDDFT computations, where we use time steps of 0.24 fs for solving the time-dependent Kohn-Sham equations. Within these calculations, we take a snapshot of the time-dependent density of states projected on the equilibrium ground-states after each five-time steps. Integration of these curves close to the Fermi energy gives the time-dependent hole concentration.

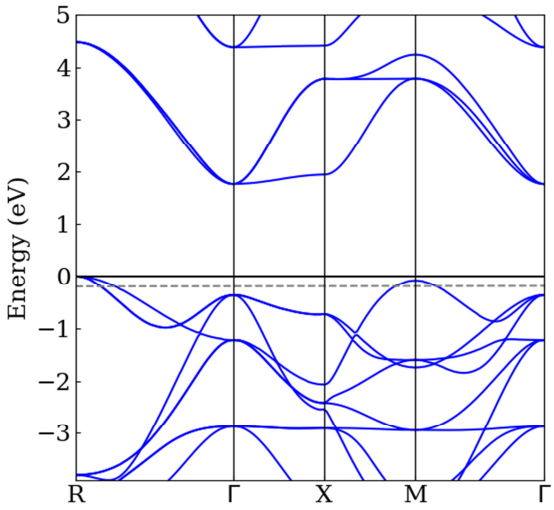

Figure S5 Band structure of cubic $SrTiO_3$ as calculated via the elk FP-LAPW code. The dashed horizontal line indicates the integration range for ρ(t) induced by the TDDFT field pulse. Please note that the Fermi energy corresponds to 0 eV.

7. Simulated dynamics including x-ray and laser parameters

To account for the mismatch in the experimental excitation and probe profiles, we calculate $u^2(t)/u_0^2$ for a series of layers from the surface into the bulk crystal with depth-dependent doping given by the excitation profile. We then superimpose $u^2(t)/u_0^2$ of the individual layers weighted by the x-ray probe profile [34]. Furthermore, we account for the experimental x-ray pulse duration by convolution with a Gaussian (FWHM 120 fs). Figure S6 shows the resulting transient intensities for selected fluences used in the experiment.
We note that strongly damped coherent oscillations of u(t) (Fig. 4) do not transfer to the resulting transient intensity due to the superposition of various oscillation frequencies given by the layer dependent excitation intensity / soft mode frequency.

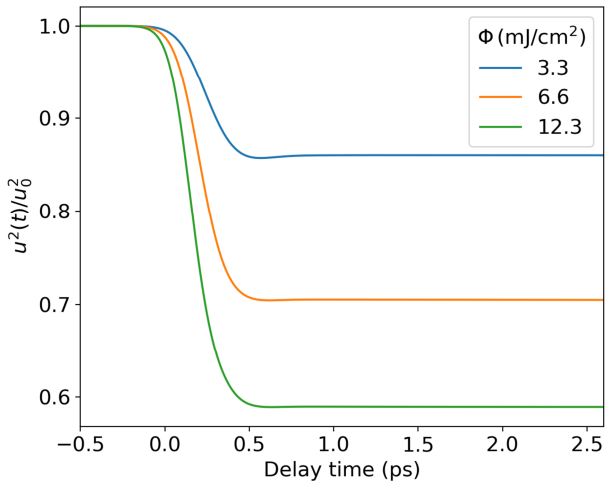

Figure S6 Simulated dynamics of the normalized intensity of a superlattice reflection taking into account the penetration depth of the pump intensity (18 nm), the x-ray probe depth (60 nm) and x-ray pulse duration (120 fs).